Stanley Geothermal Feasibility Study

Task 4 Report: Geologic and Geophysical Surveys

Kyle Makovsky
Boise State University
Department of Geosciences
1910 University Drive
Boise, ID 83725
KyleMakovsky@u.boisestate.edu
Phone: 208-473-8633

Leland "Roy" Mink
Mink GeoHydro Inc
H2oguy@copper.net
Phone: 208-699-4396

Robert Beckwith
2260 Dicky Ct.
Eagle, ID 83616
bobbeckwith@qwest.net
Phone: 208-939-8936

December 1, 2011

1. Introduction

Three surveys were conducted in the Stanley area in the months of September, October, and November of 2011 to help characterize the geothermal system near Stanley. A resistivity and gravity survey, both of which are geophysical methods, and a shallow probe (2 meter survey), which is a geological method that measures shallow subsurface heat flow, were conducted. The gravity survey was conducted by students and faculty from Idaho State University and the resistivity survey was conducted by students and faculty of Idaho State University in conjunction with scientists from Idaho National Laboratory.

2. 2 Meter or Shallow Probe Survey

2 meter surveys have become increasingly popular in geothermal exploration because they are relatively inexpensive and can yield important information on heat flow resulting from upflow zones of hydrothermal waters. Soil temperatures will be higher where hydrothermal water migrates to the surface through fault or fracture systems. These are referred to as upflow zones and can be measured with 2 meter probes.

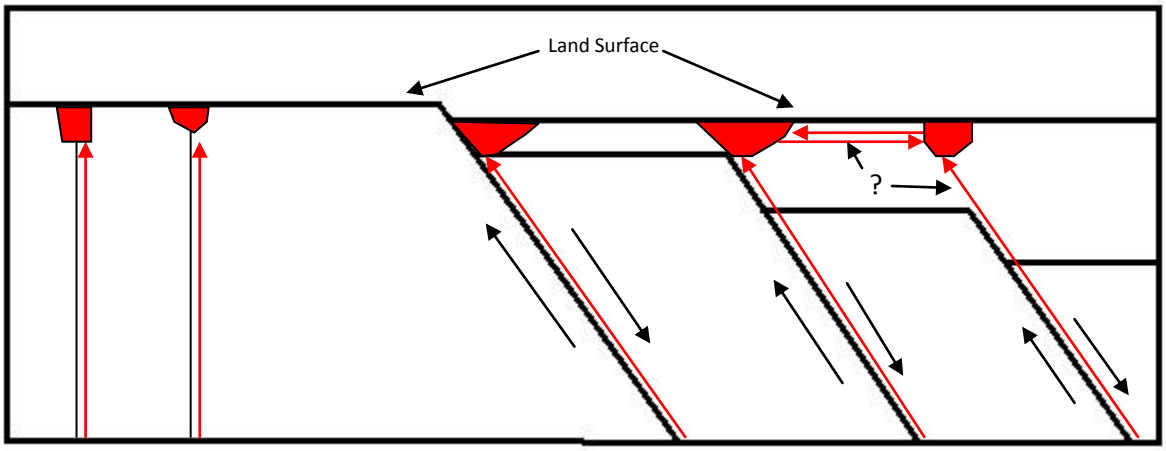

Figure 1. Schematic diagram showing 2 potential scenarios for thermal water upflow. Thin lines on left side of diagram represent fractures that could be present in any rock formation. Lines dipping to the right on the right side of diagram represent faults with arrows showing relative slip motion. Red lines with arrow tips represent movement direction of thermal water and red areas represent areas where soil temperatures have potential to be higher due to upwelling of thermal waters. Farthest right heat anomaly has 2 potential sources, one from lateral migration of thermal water or also from upflow of thermal waters along the fault, or a combination of these two processes. Not to scale.

Depths of 2 meters (~6 ft) are chosen because at this depth daily fluctuations in temperature are not recorded (Sladek, 2007); although seasonal variations are still measured. This method has been described in detail by Sladek et al (2007), Coolbaugh et al (2007), and Kratt et al (2008). The method has been applied and tested against structural and thermal gradient data and has been used to locate blind geothermal systems in Nevada. The probes are made of hollow steel pipes with a carbon hardened tip

at the lower end. They are driven into the ground with an electric (Milwaukee) heavy drill powered by a (Honda) generator with approximately 6 inches left exposed above ground. This upper 6 inches is insulated with a Styrofoam cover to minimize solar conduction into the steel rod. After 24 hours, the pipe is considered to be in thermal equilibrium with the surrounding soil. The temperature is measured by inserting a thermister into the hollow portion of the pipe, and after 5 minutes the temperature is recorded. During these 5 minutes the thermister has equilibrated with the pipe and surrounding soil.

The survey in Stanley placed a total of 24 shallow probes located on both private and public lands, mostly within or northeast of Stanley. The locations of the 24 probes were established to gather shallow thermal gradient data on the valley floor between Upper Stanley and Lower Stanley. Also, mapped faults and/or lineaments were considered when placing probes, as we wanted to establish several profiles that cross cut these fault traces, because they may serve as conduits for geothermal fluid movement (figure 1). Also a number of probes were established in the area of thermal spring discharge north of Stanley in the area of the confluence of Valley Creek and the Salmon River. Figure 2 shows these locations as well as the temperature measured at each site. Table 1 lists the xy coordinates as well as measured probe and air temperatures.

Probe #	Easting	Northing	ProbeTempF	AirTempF
0	666830	4900484	49	28.9
1	666929	4900390	55.1	35
2	667010	4900239	50.8	59.7
3	667078	4900187	49.6	65.5
4	666440	4899487	53.7	63
5	666396	4899573	51.4	62.6
6	666273	4899678	50.4	63
7	665232	4898924	56.2	64.3
8	665225	4898215	57.3	51.7
9	665238	4898479	59	55.4
10	665495	4898790	64.4	37.9
11	665011	4898491	54.7	65.6
12	665495	4898790	51.1	72.4
13	665548	4898926	52.5	67.1
14	665538	4899204	55.6	60.4
15	665958	4898937	55.1	61.9
16	665794	4898960	52.4	57.8
17	664757	4898107	49.1	68.3
18	664329	4898216	54.6	71.1
19	665712	4897356	54.4	38.7
20	665607	4897337	52	42.3
21	665433	4897378	50.8	44
22	664842	4898267	55.8	57.2
23	664776	4898264	53.3	50.8

Table 1. UTM coordinates for measured stations in the Stanley area (NAD83). A total of 24 stations were measured, with an average temperature of 53.7° F.

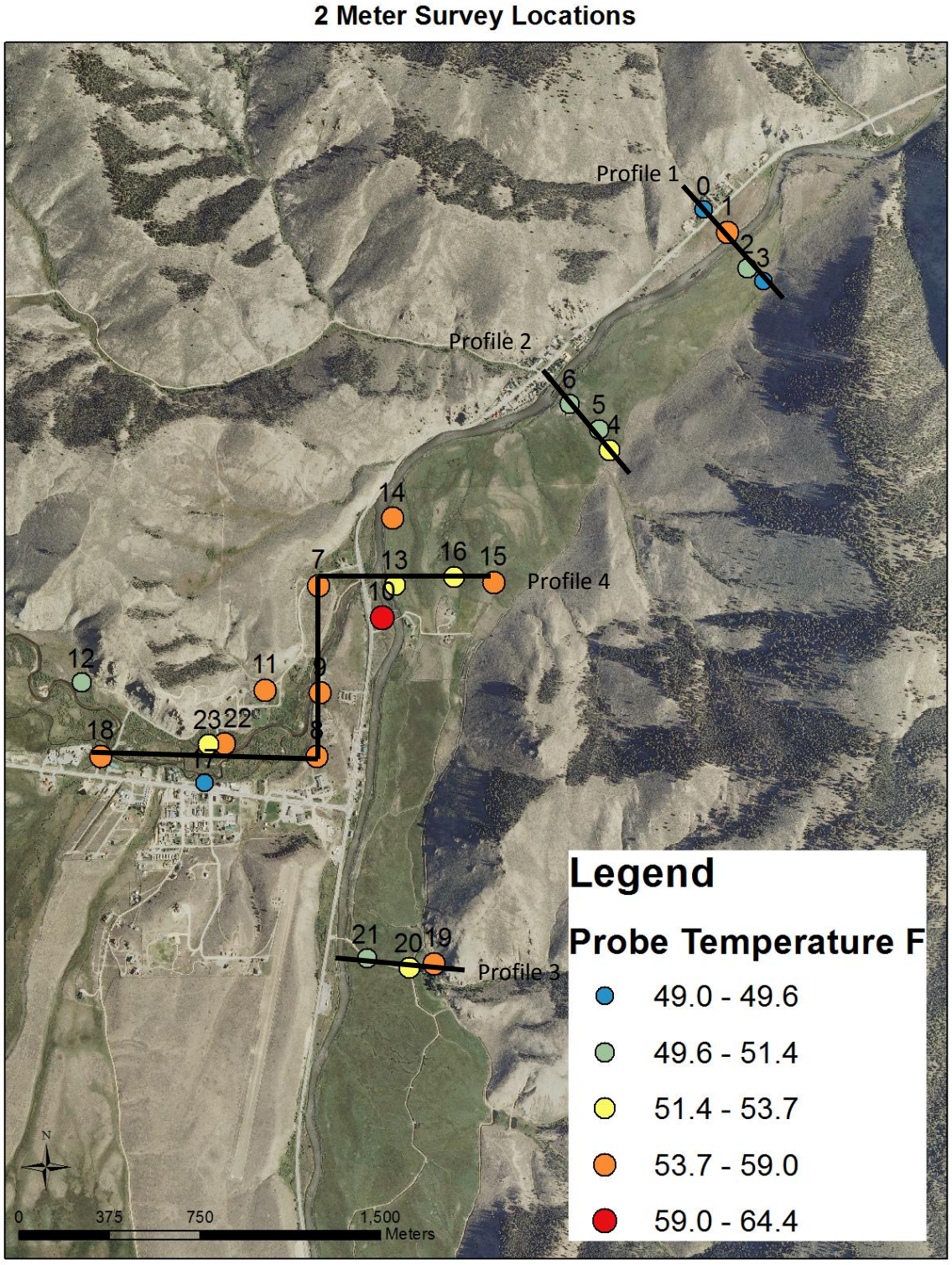

Figure 2. Map of Stanley area showing locations of 2 meter probes. Probes were placed at strategic locations, and four profiles were created to try and better understand the role of local faults on thermal water movement, see text for a more detailed description.

Two northwest-southeast profiles were created in the northeastern section of the survey area (figure 2). The northeastern most profile (Profile 1, figure 2,) yielded temperatures in the range of 49°-59° with the highest temperature measured at station 1. The profile with stations 4-6 (Profile 2, figure 2) shows temperatures in the range of 49.6°-53.7°. The profile containing stations 19-21 (Profile 3, figure 2) range in temperatures from 49.6°-59° and progressively gets cooler stepping away from the range-front. A fourth profile (Profile 4, figure 2) has been created that starts from west to east, with stations 18, 23, 22, 8, 9, 7, 13, 16, and 15. This profile illustrates the measured temperatures of the warmest part of the survey area. Graphical representations of these profiles can be seen in figure 5. For further illustration, a contour map of the 2 meter survey results was created and can be seen in figure 4. From this contour map and from profile 4, it is apparent that the warmest measured stations all lie near the confluence of Valley Creek and the Salmon River. All of these points have measured temperatures within 53.7°-59°. Figure 3 shows the distribution of stations with measured temperatures separated in 2° intervals. The highest frequency of measured temperatures lie within the 54°-56° range.

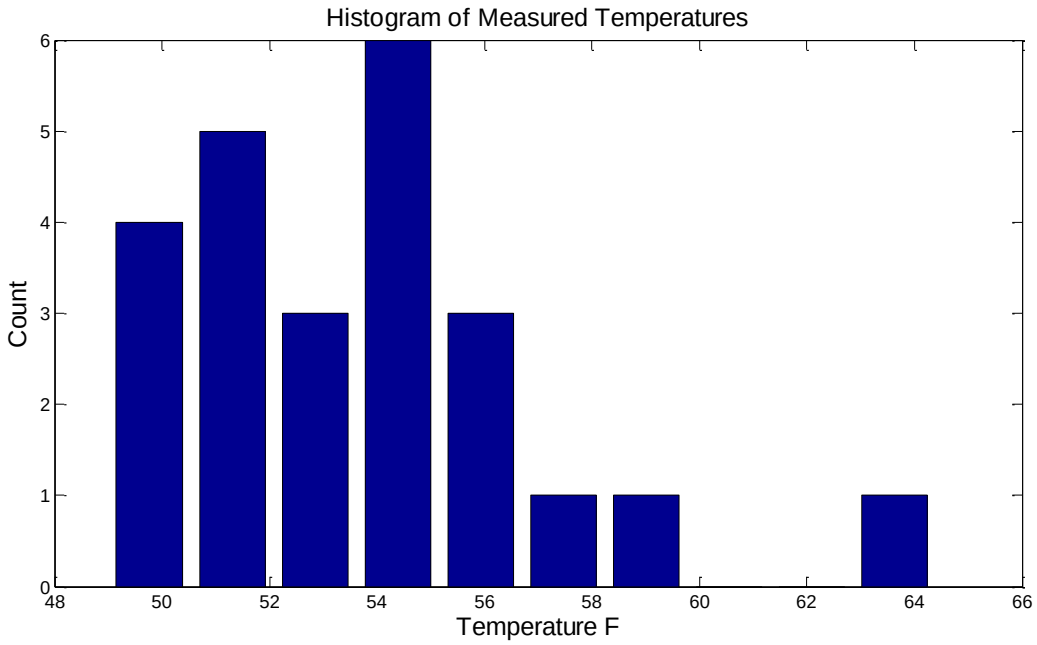

Figure 3.

Profiles 1 and 2 show anomalously low temperatures possibly due to the fact that they were driven near areas where excessive irrigation have created man made bogs (figure 6). These bogs would effectively reduce the signal of potential upwelling thermal water. The increase in temperature moving eastwards across profile 3 could be due to upwelling of thermal water along the fault bounded range-front. The area near the confluence of Valley Creek and the Salmon River show the highest temperatures, as mentioned above. This result is in agreement with temperatures measured from several warm water seeps and hot springs in this area, measured by students of Idaho State University (Students and Faculty of Idaho State University, written communication, 2011). Though not all of these seeps are high temperature, the majority (~10) are above 26.8° Celsius.

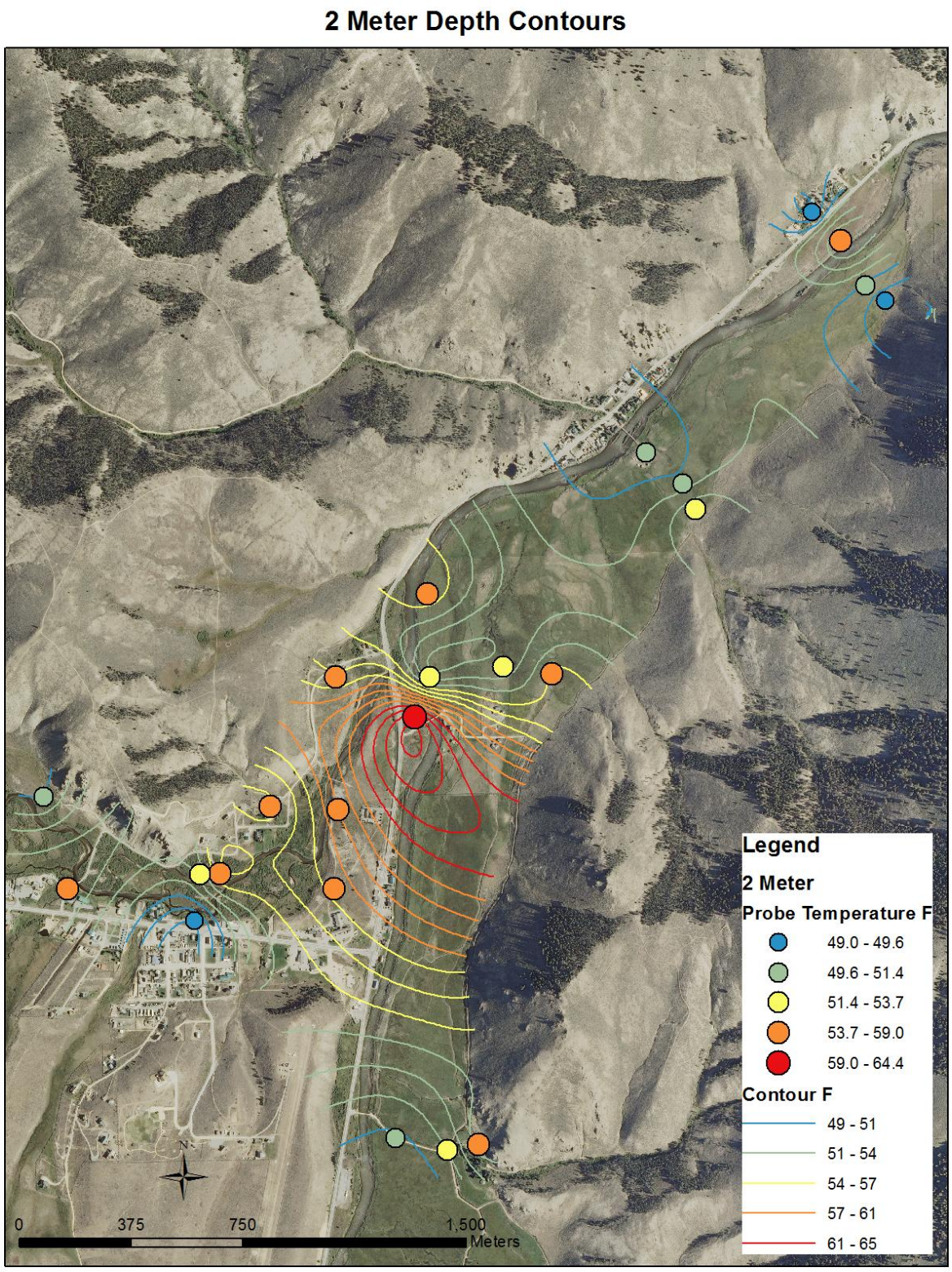

Figure 4. Map of 2 meter locations and also of contours created from 2 meter temperatures. The main area of potential based on this shallow gradient data is near the confluence of Valley creek and the Salmon River.

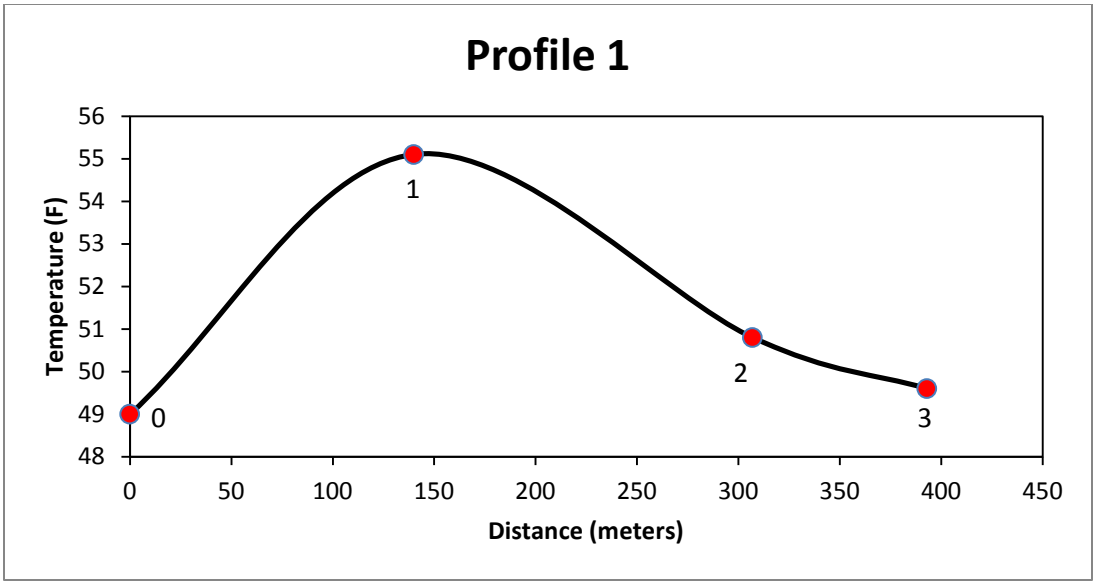

Figure 5a. Graphical representation of temperature vs probe number for profile 1. See figure 2 for location. Probe 1 has the highest measured temperature along this profile. Numbers next to points represent probe number.

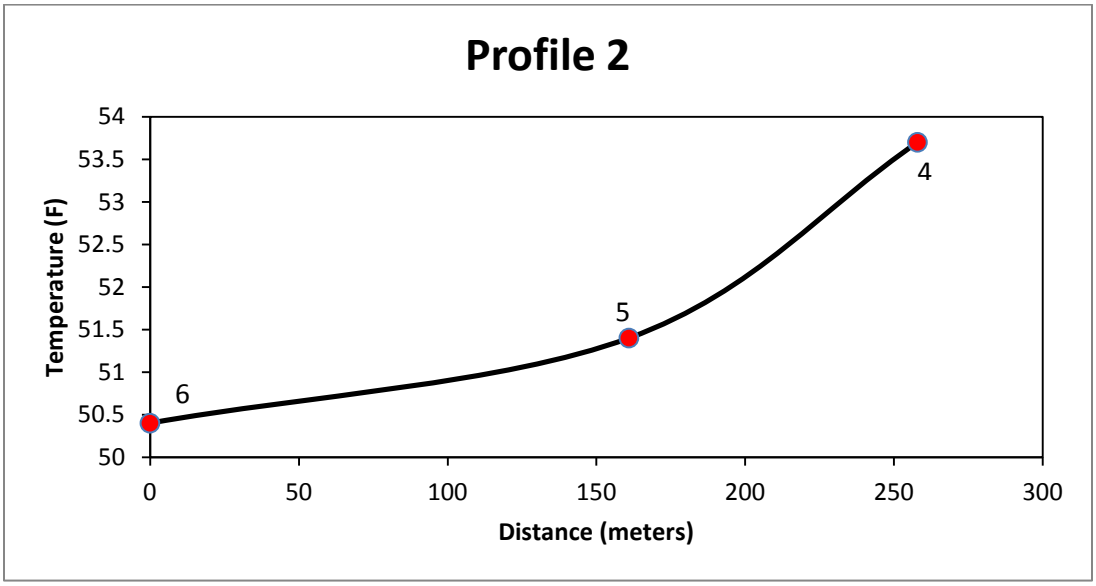

Figure 5b. Graphical representation of temperature vs probe number for profile 2. See figure 2 for location. Probe number four has highest measure temperature along this profile, most likely because it is not located within a boggy area (see text). Numbers next to points represent probe number.

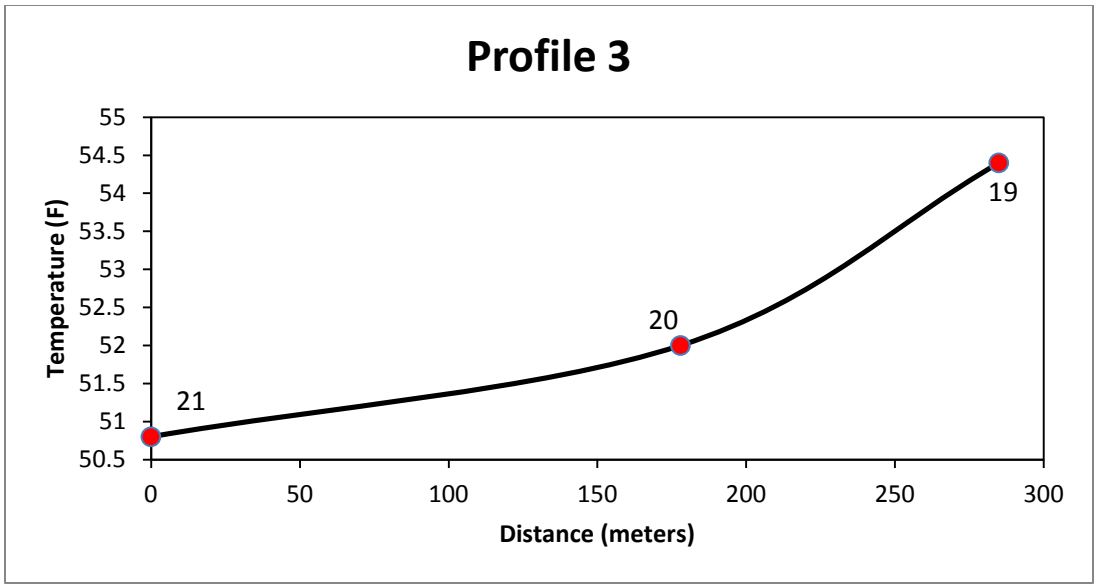

Figure 5c. Graphical representation of temperature vs probe number for profile 3. See figure 2 for location. Probe 19 is located near a fault that bounds the eastern side of the Stanley Basin. This fault could potentially have thermal waters that are flowing upwards. Numbers next to points represent probe number.

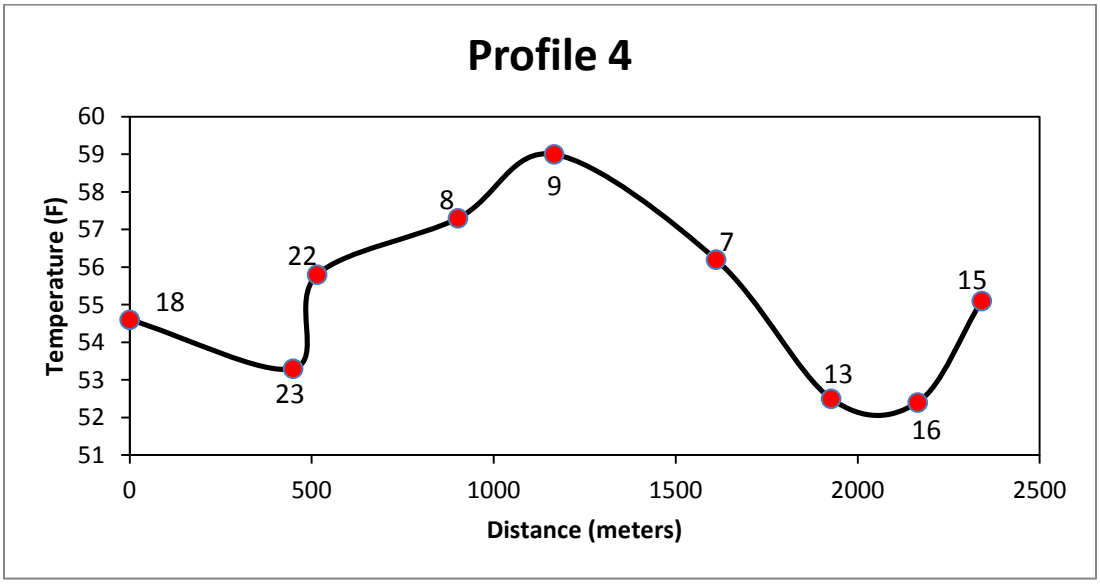

Figure 5d. Graphical representation of temperature vs probe number for profile 4. See figure 2 for location. This area has the highest mean temperatures of the entire study area. See text for further discussion. Numbers next to points represent probe number.

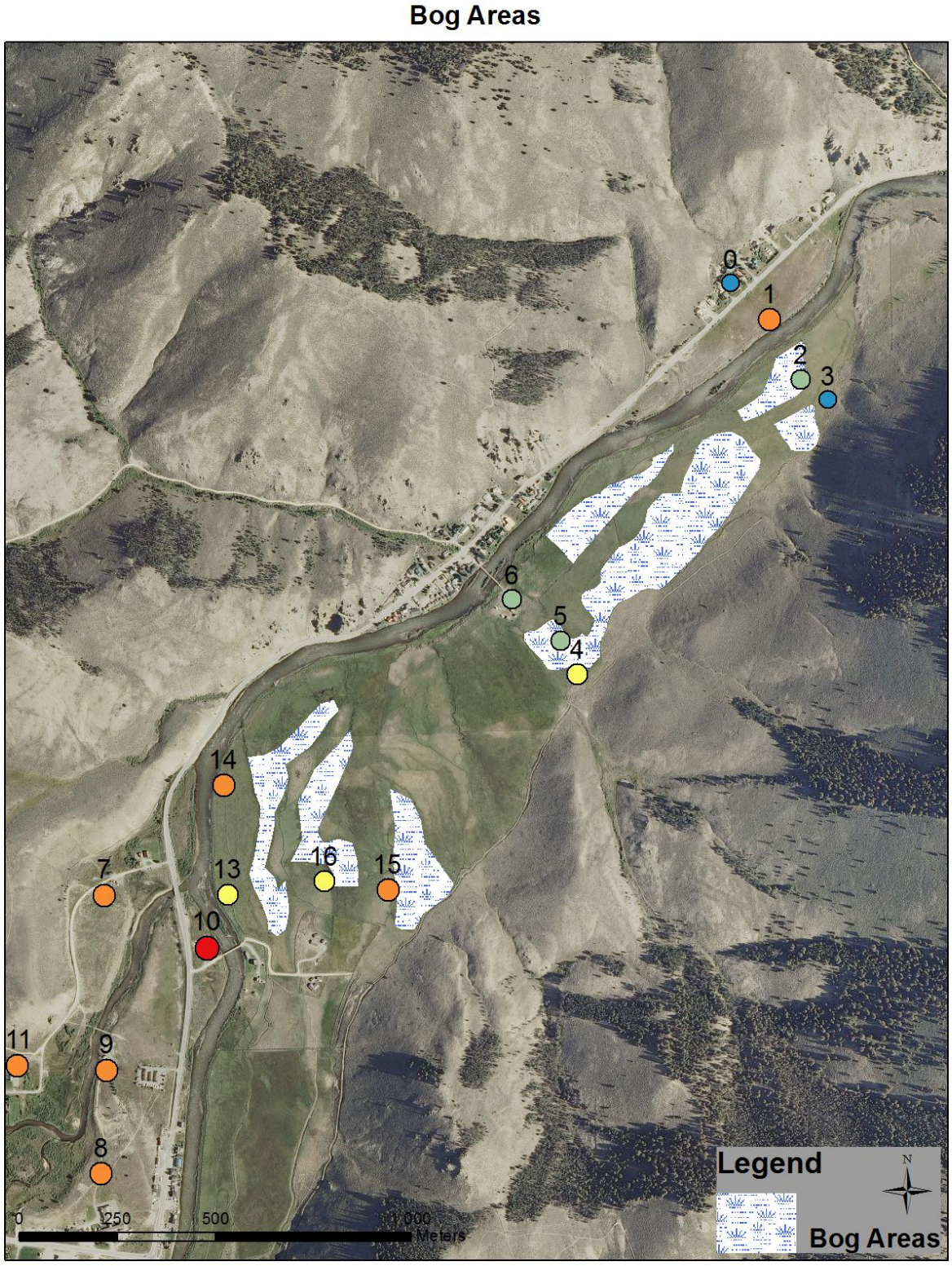

Figure 6. Locations of bogs mentioned in text. These could be significant because they would effectively mask zones of upwelling thermal water from the 2 meter probes.

3. Gravity Survey

Gravity surveys measure the change in Earth's gravitational field due to changes in density and relative offset by geologic structures. The geometry of geologic structures can also be ascertained by gravitational measurements. The device used for such a survey is called a gravimeter and uses a highly sensitive quartz spring to measure gravitational potential. There are several influences on the value of gravity measured by the gravimeter such as: the elevation of the station measured, the latitude of the station, the weight of the overlying atmosphere, tidal effects from the gravitational attraction of the Moon, and the terrain of the surrounding area, these will be discussed in further detail later. For geologic purposes we are only interested in changes in density and geometry produced by geologic structures (i.e. faults).

The gravity survey for the Stanley project consists of 10 stations and one base station. The use of a Worden Gravity Meter requires the reoccupation of a base station site once every 2-3 hours (Holom and Oldow, 2007). This reoccupation allows for the correction of meter drift to be calculated. A profile was created north of Stanley to try and capture the geometry of potential faults that exist underneath the Stanley Basin (figure 7).

As mentioned above, several factors affect measured gravity values at any given point, therefore several corrections must be applied to the raw data in order to produce meaningful results. The method used for the Stanley survey followed the data reduction process of Holom and Oldow (2007). A brief description is provided here along with the equations used for the raw data reduction process.

Any point on the Earth's surface has a theoretical gravitational value based on that locations latitude, the formula for calculating this value is, in mGals (Holom and Oldow, 2007; Moritz, 1980; Hildenbrand et al, 2002):

$$g_\phi = g_e \times ((1 + k \sin^2 \phi) / (1 - e^2 \sin^2 \phi)^{1/2}),$$

where g_e = 978032.67715 mGal, k and *e* are dimensionless coefficients (see Holom and Oldow, 2007) and the units of g_ϕ are in mGals (1 m/s^2 = 100,000 mGals).

The mass of the atmosphere also plays a direct role in observed gravity values, this is corrected for by the equation (Holom and Oldow, 2007; Hildenbrand et al, 2002):

$$g_{atm} = 0.874 - (9.9 \times 10^{-5} h) + (3.56 \times 10^{-9} h^2),$$

where *h* is the height of the gravity station in meters above the GRS80 ellipsoid (Holom and Oldow, 2007).

There is also a correction needed for the elevation of the gravity station because as distance from the center of the earth increases, the value of measured gravity will decrease (Holom and Oldow, 2007).

$$g_h = -(0.3087691 - 0.0004398 \sin^2 \phi) h + (7.2125 \times 10^{-8}) h^2,$$

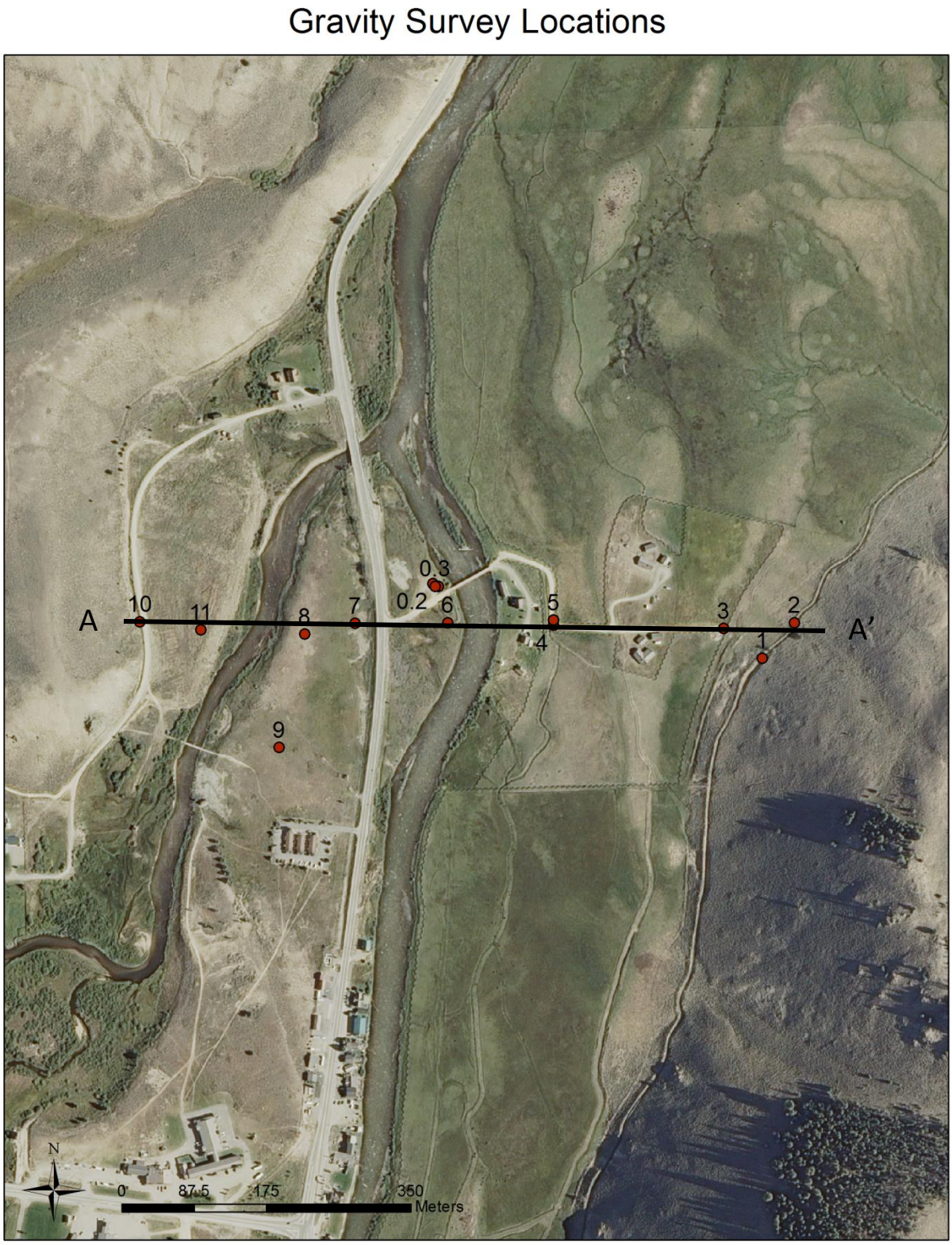

Figure 7. Locations of gravity survey locations along profile A-A'.

'where *h* is the height of the gravity station in meters above the GRS80 ellipsoid and ϕ is the latitude of the gravity station (Holom and Oldow, 2007).'

The Bouguer Spherical Cap correction accounts for the mass that is in between the gravity station and the reference ellipsoid (GRS80) and can be calculated with the equation (Holom and Oldow, 2007; LaFehr, 1991, Hinze, 2003; Hildenbrand et al, 2002):

$$g_{sc} = 2\pi G\rho(\mu h - \lambda R)$$

where G Newton's gravitational constant, ρ is the density of material (in kg/m^3), μ and λ are dimensionless coefficients, *h* is the height in km above the reference ellipsoid (GRS80), and R is the combined height of the gravity station and average radius of the Earth in km (Holom and Oldow, 2007).

The final correction made is the terrain correction (g_{tc}). This correction takes into account the terrain of the surrounding area, as they can affect the gravity of a point up to 50 km away (Shaun Finn, pers. com., 2011). This correction was prepared by importing a 30 meter resolution Digital Elevation Model downloaded from the USGS National Seamless Server. Next, a grid of points was created with spacing of 2.5 km in ESRI's ArcGIS software (figure 8). Easting, northing, and elevation data was assigned to these points using various tools provided in ArcGIS. This information was then entered into a MATLAB code that calculates the value of the terrain correction.

After each individual correction has been calculated, the complete Bouguer Anomaly for each point is calculated by (Holom and Oldow, 2007):

$$\Delta g = g_{obs} - (g_{\phi} + g_h - g_{atm} + g_{sc} - g_{tc})$$

The results of the gravity data reduction is listed in table 2 below. The values of the Complete Bouguer Anomaly value range from -213.82 to -211.92 mGals. The cross sectional view from the measured gravity values is represented in figure 8, moving eastward from left to right. A conceptual structural model based on interpretations of the gravity data is located on the bottom portion of figure 9. The gradual increase in gravity values on the left side of the diagram is interpreted as being a thickening of alluvial sediments adjacent to a down-dropped block created by a normal fault. The sharp decrease in gravity is interpreted as being a down to the east block of crust created by a normal fault. A dramatic decrease in gravity values is observed near the easternmost part of the profile, interpreted as a juxtaposition of less dense basin fill adjacent to relatively more dense granitic bedrock also created by movement on a normal fault.

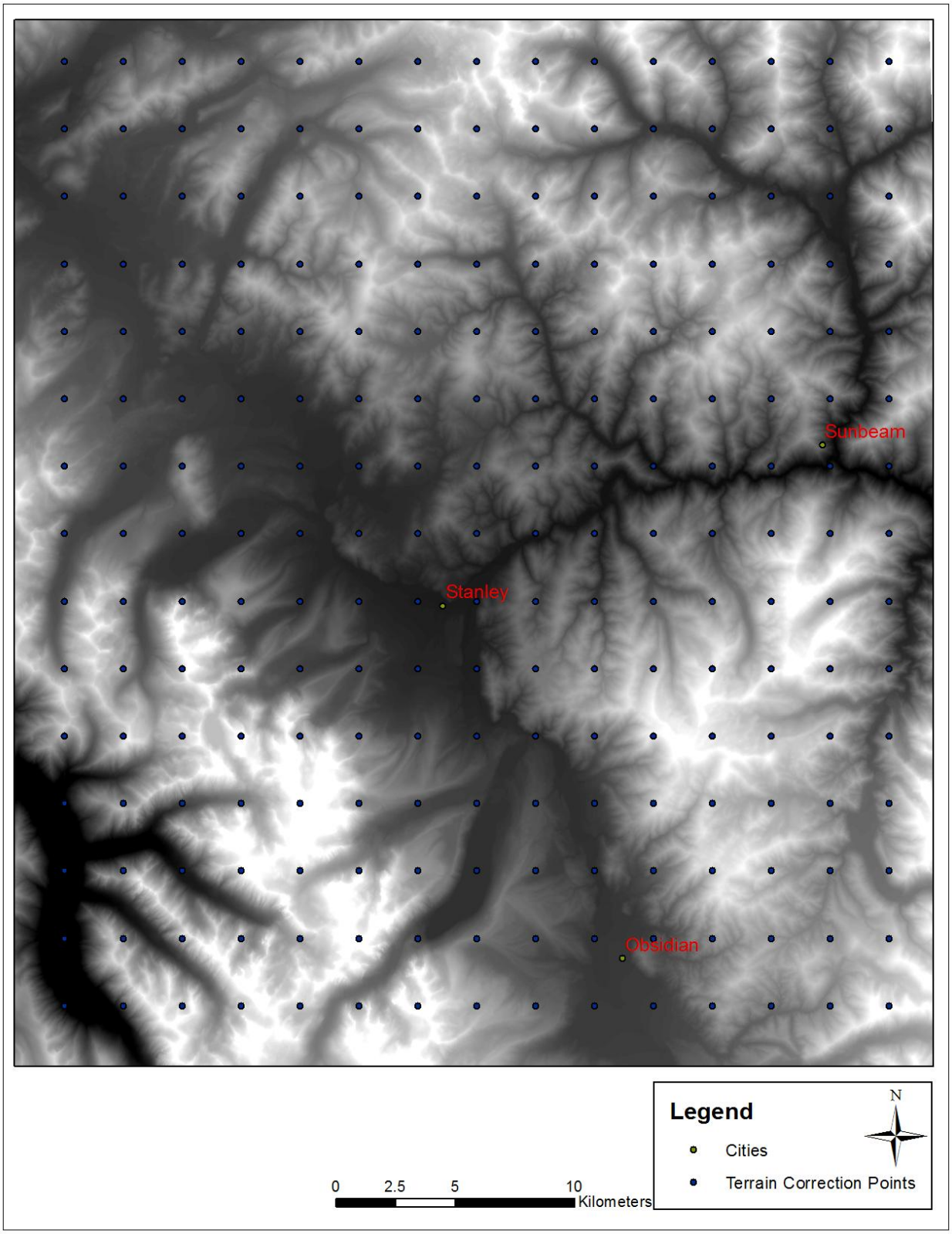

Figure 8. Locations of points used in calculating the effect of local terrain on the Bouguer Anomaly near Stanley. X,Y, and Z data is needed for all points in this figure to make that calculation.

Station Number	Easting Coordinate (m)	Northing Coordinate (m)	Elevation (m)	Complete Bouguer (mGals)
Base 1	665157	4898731	1901.6	-213.24
1	665231	4898721	1898.4	-212.97
2	665326	4898579	1905.2	-213.07
3	665357	4898716	1902.4	-212.60
4	665418	4898729	1901.6	-212.62
5	665512	4898777	1896.0	-212.97
Base 2	665157	4898731	1901.6	-213.28
6	665519	4898774	1895.9	-212.96
7	665658	4898730	1896.6	-212.96
8	665658	4898727	1898.7	-212.91
9	665864	4898733	1898.7	-212.57
Base 3	665157	4898731	1901.6	-211.92
10	665911	4898687	1911.3	-213.45
11	665950	4898730	1910.1	-213.82

Table 2. UTM coordinates, elevations, and the calculated Bouguer Anomaly value of each gravity station for the Stanley survey.

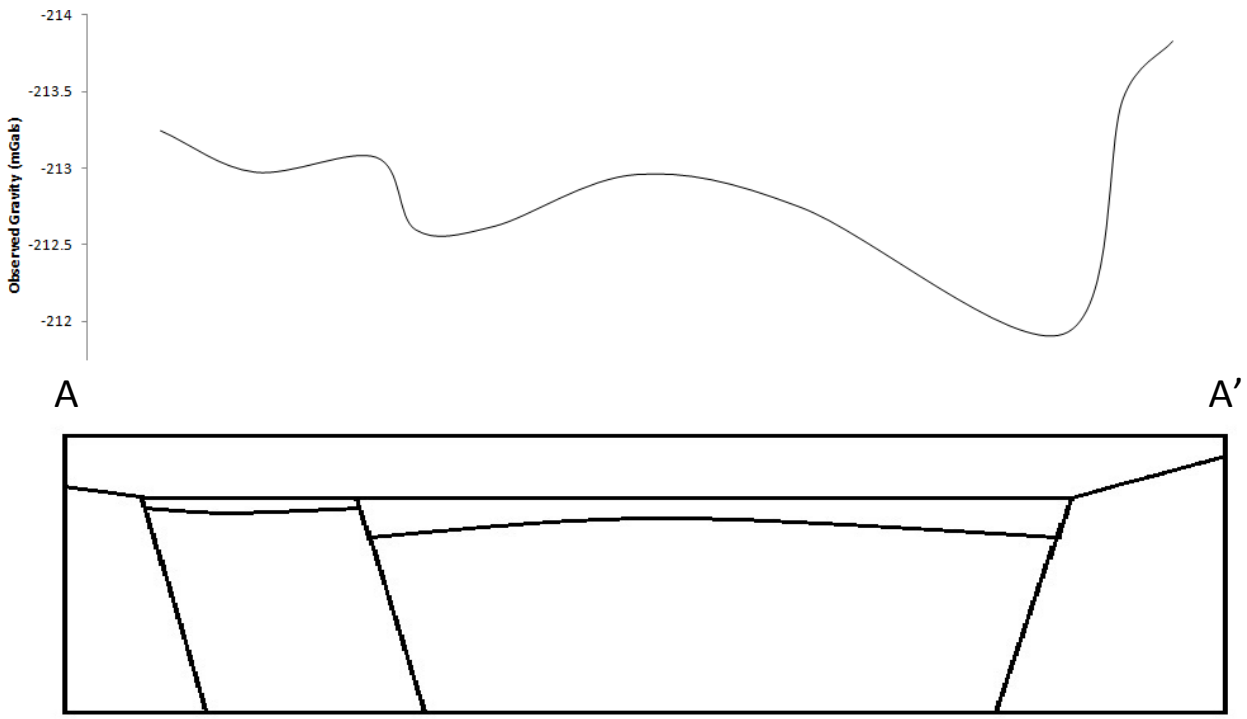

Figure 9. Conceptual and schematic cross section based on interpretations of the gravity profile. Major changes in the Bouguer Anomaly are interpreted as the juxtaposition of less dense basin fill sediments against relatively more dense bedrock of the Idaho batholith.

4. References

Coolbaugh, M.F., Sladek, C., Faulds, J. E., Zehner, R.E., Oppliger, G.L. 2007. Use of Rapid Temperature Measurement At A 2 Meter Depth to Augment Deeper Temperature Gradient Drilling. Proceedings, 32nd Workshop on Geothermal Reservoir Engineering. Stanford University, Stanford, California.

Hildenbrand, T.G., Briesacher, A., Flanagan, G., Hinze, W.J., Hittelman, A.M., Keller, G.R., Kucks, R.P., Plouff, D. 2002. Rationale and Operational Plan to Upgrade the U.S. Gravity Database. USGS Open File Report 02-463. 12 p.

Hinze, W.J., Aiken, C., Brozena, J., Coakley, B., Dater, D., Flanagan, G., Forsberg, R., Hildenbrand, T., Keller, G.R., Kellogg, J., Kucks, R., Li, X., Mainville, A., Morin, R., Pilkington, M., Plouff, D., Ravat, D., Roman, D., Urrutia-Fucugauchi, J., Veronneau, M., Webring, M., Winester, D. 2003. New Standards for reducing gravity observations: The Revised North American Gravity Database: http://paces.geo.utep.edu/research/gravmag/PDF/Final%20NAGDB%20Report%20091403.pdf

Holom, D.I., Oldow, J.S. 2007. Gravity reduction spreadsheet to calculate the Bouguer anomaly using standardized methods and constants. Geosphere. v. 3, no. 2. p. 86-90. doi: 10.1130/GES00060.1. 1 Figure. 4 spreadsheets.

Kratt, C., Coolbaugh, M., Sladek, C., Zehner, R., Penfield, R., Delwiche, B. 2008. A New Gold Pan for the West: Discovering Blind Geothermal Systems with Shallow Temperature Surveys. Geothermal Resources Council, Transactions. vol. 32.

LaFehr, T.R. 1991. An exact solution for the gravity curvature (Bullard B) correction. Geophysics. v. 56, no. 8. p. 1179-1184. doi: 10.1190/1.1443138.

Moritz, H. 1980. Geodetic reference system. Journal of Geodesy. v. 74. p. 128-162.

Sladek, C., Coolbaugh, M.F., Zehner, R.E. 2007. Development of 2-Meter Soil Temperature Probes and Results of Temperature Survey Conducted at Desert Peak, Nevada, USA. Geothermal Resources Council Transactions. v. 31. p. 363-368.